Structures 65 (2024) 106728

Contents lists available at ScienceDirect

Structures

journal homepage: www.elsevier.com/locate/structures

Non-stationary winds effects over large partially-open roofs: A CFD study regarding the role of unsteady aerodynamics

Jin Xing, Luca Patruno *, Stefano de Miranda, Francesco Ubertini

DICAM, University of Bologna, Viale del Risorgimento 2, 40136 Bologna, Italy

ARTICLE INFO

Keywords:
Unsteady aerodynamics
Non-stationary wind
Downbursts
Large-span roofs
Large Eddy Simulation

ABSTRACT

Non-stationary winds are increasingly attracting the attention of the scientific community and, despite not being explicitly considered in current design practice, they are known to produce important damages. In particular, the non-stationarity of such events has important consequences with respect to four main aspects which affect the definition of design wind loads: (i) the design wind speed definition, (ii) the wind profiles, (iii) the calculation of the structural response and (iv) the insurgence of unsteady aerodynamics effects. While the first three aspects already received considerable attention, the last one is still largely unclear and its relevance still to be assessed. In particular, for non-stationary winds such as macro- and micro-downbursts, the ramp-up time might become so short to trigger unsteady aerodynamic effects in the overall flow arrangement, which cannot be inferred from results obtained for stationary cases. In this paper, we propose a first investigation of such matter considering a large stadium roof using Large Eddy Simulations. Results show that, for the considered case, noticeable unsteady aerodynamic effects, which leads to an amplification of wind loads, can be triggered when the wind rump-up time is in the order of 30 s, and quickly decrease in importance for higher rump-up times.

1. Introduction

The role played by non-stationary winds in the definition of design loads has been well-known for a long time and it is increasingly attracting the attention of the scientific community. Numerous aspects distinguish such events from stationary winds, on which currently available standards and codes are based [1–3].

In particular, it is possible to identify four main aspects which differentiate such winds from stationary ones: the design wind speed definition, the wind profiles, the calculation of the structural response and the insurgence of unsteady aerodynamic effects.

As regard the first aspect, first contributions regarding the necessity to classify meteorological events and provide separate probability distributions for extreme wind speeds caused by each of them can be traced back to [4,5]. The problem assumes even more relevance if the representativeness of the 10 min average wind speed is questioned, on which numerous standards, Eurocode included, are based [6].

Regarding the second aspect, it is well-known that non-synoptic winds can be characterized by unusual profiles of the time-averaged wind speed (as well as other relevant quantities such as turbulent intensity and length scales) with respect to the logarithmic or power-law ones, usually adopted to represent the Atmospheric Boundary Layer, ABL [7–10]. In particular, in the case of downbursts, the vertical distribution of the mean wind speed is well-known to exhibit a nose-shaped profile, resulting in wind loads which differ from those induced by stationary winds. The mechanisms underlying the generation of such nose-like shape is generally clear, but the matter is still the object of numerous investigations [9,11].

Coming to the calculation of the structural response, for non-stationary winds, the impulsive nature of the excitation might become important when the evolution time of the phenomenon [12] is comparable to the lowest structural mode period (see for instance [13,14]). In such conditions, the assumption of stationary response shall be abandoned, and appropriate methodologies adopted for the evaluation of the structural response.

The above summary is extremely limited and not exhaustive, but it provides an overview of the peculiarities which differentiate stationary and non-stationary winds, as far as the evaluation of wind loads assessment is concerned. Reference is made to [15,16] for further details and to [9,17,18] for a comprehensive treatment of such aspects in the case of high-rise buildings or to [19] for the case of bridge decks aerodynamics.

As anticipated, in addition to the aforementioned differences, a fourth aspect shall be added: the role played by unsteady aerodynamic effects in the overall flow arrangement. In particular, sudden variations

* Corresponding author.
E-mail address: luca.patruno@unibo.it (L. Patruno).

https://doi.org/10.1016/j.istruc.2024.106728
Received 28 December 2023; Received in revised form 7 May 2024; Accepted 7 June 2024
Available online 13 June 2024

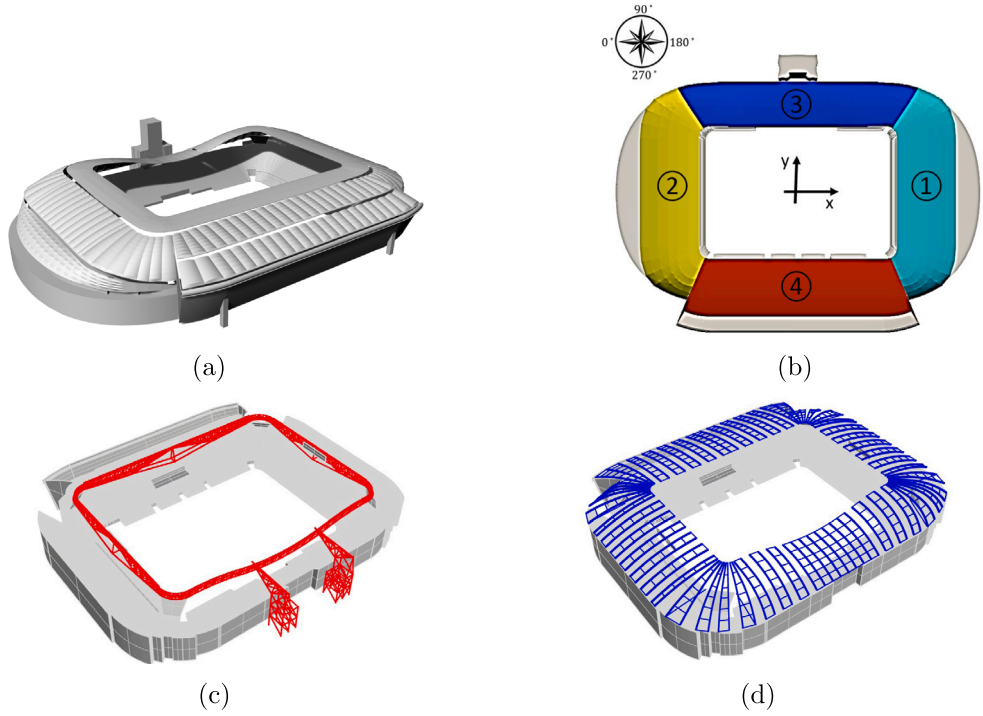

Fig. 1. The Bologna stadium: (a) overview, (b) the roof subdivision into sectors, (c) the primary structures and (d) the secondary structures. *Source:* Adapted from [29].

of the incoming wind speed or incidence angle, might trigger an unsteady response of the overall flow organization, which cannot be deduced by inspecting the response to stationary winds. In particular, shear layers, which are often the dominant feature defining the flow around bluff bodies, are known to lead to delayed responses, with direct effects on the generated aerodynamic forces [20–22] and, potentially, over-shootings [23]. The problem can be summarized as follows: for stationary (slowly varying) winds, it can be assumed that the maximum wind speed is reached gradually so that, overall, the flow around the structure has sufficient time to adjust to the increasing velocity, so to say, in a quasi-static manner. We remark that the term quasi-static is here adopted slightly inappropriately, referring exclusively to the slowly varying modifications of the overall flow arrangement, excluding its unsteady turbulent components or any unsteady local flow mechanisms occurring at short time-scales. Conversely, non-stationary winds might exhibit strong variations in a very limited time, so that the slowly-varying mean flow varies too quickly to be treated in a quasi-static way. In the following, despite such consideration, we will keep denoting it as slowly-varying mean flow.

The topic, similar to well-known problems found, for instance, in aeroelasticicty [24,25] and accelerating flows [26,27], assumes particular connotations in the field of non-stationary winds, which remain largely unexplored [21].

The matter, sometime also denoted as non-stationary (or transient) aerodynamic wind loading [28], currently represents a strong source of uncertainty in the evaluation of the wind actions induced by non-stationary winds.

In this paper, to shed light on such matter, we consider a typical stadium roof, already studied in stationary wind conditions using Large Eddy Simulations, LES, in [29]. In fact, based on previous observations, unsteady aerodynamic effects are expected to become relevant when the wind ramp-up time becomes comparable to the characteristic time-scale of the flow, the latter one being proportional to the immersed structure length-scale. For long-span bridges, while being the overall length-scale extremely large, the time-scale is actually proportional to the characteristic dimension of the constitutive elements cross-sections (i.e. deck, towers and cables), resulting in relatively short time-scales. In contrast, partially open-roof stadia lead to very large vortical structures, and are classically characterized by a cavity flow which adapts to changes in the external flow with remarkable retard, making them potentially prone to develop unsteady aerodynamic effects.

In this study, aiming at isolating unsteady aerodynamic effects from other aspects, we deliberately neglect other peculiarities of non-stationary winds, which depend on the particular considered atmospheric phenomenon. In particular, we retain the standard logarithmic velocity profile and analyse the aerodynamic response of the roof when subjected to non-stationary winds, characterized by different ramp-up times. Then, taking as reference the aerodynamic forces measured in stationary wind conditions, we analyse the uplift acting on the roof for increasingly more impulsive gusts. The analysed cases, despite simplified, are representative of loading conditions classically observed for macro- and micro-bursts.

The paper is organized as follows. Firstly, the description of the considered structure and the adopted numerical model are reported in Section 2. Then, the generation of the non-stationary wind fields used as inflows is discussed in Section 3. The uplift generated on the roof considering different ramp-up times is compared to the value obtained in stationary conditions in Section 4 and, finally, conclusions are drawn in Section 5.

2. Case description

In this study, as a typical example of a large span stadium roof, we consider the newly designed covering for the Bologna stadium, *Stadio Renato Dall'Ara*, Italy. The roof measures 227 m and 160 m along its longer and shorter sides, respectively, and it is positioned at approximately 37 m above the ground. The roof is partially-opened, covering only parts over the stands. An overview of the stadium is reported in Fig. 1(a). An overview of the roof subdivision into sectors and the structural system is provided in Fig. 1(b), (c) and (d). Further details regarding the structural system, not relevant for the present investigation, can be found in [29].

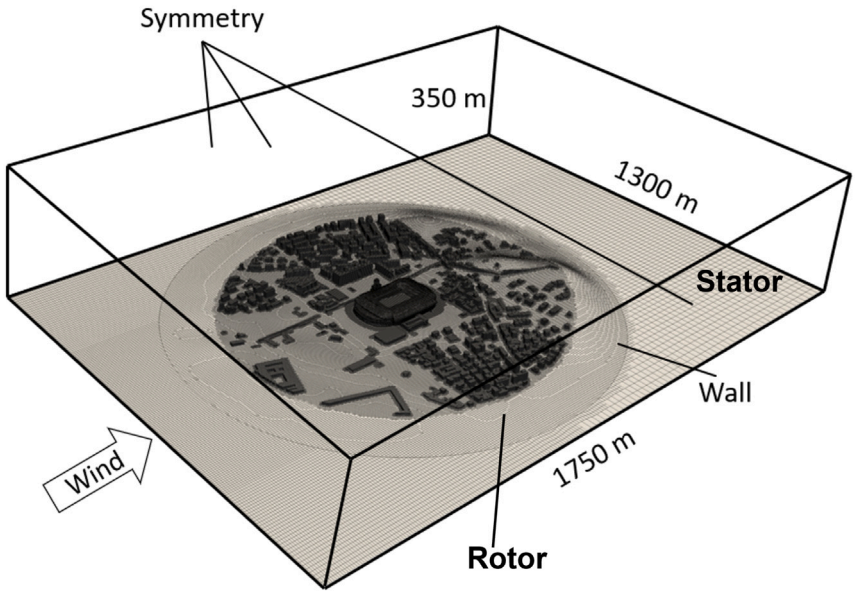

Fig. 2. Overview of the computational domain, boundary conditions and mesh.

The stadium has been recently studied using LES in [29], considering the effect of stationary winds. Briefly, the stadium surrounding have been reconstructed for a radius of 450 m and the overall adopted computational domain measures 1750, 1300 and 340 m in the along-wind, cross-wind and vertical directions, respectively.

Simulations have been performed in full-scale, but the fluid viscosity has been increased of a factor 300 to decrease the Reynolds number, making it comparable to wind tunnel tests performed on reduced-scaled models with a length scaling factor equal to 1/300. The Reynolds number based on the roof height (i.e. 37 m) and the reference velocity in the stationary case (i.e. 27 m/s) is approximately 2.94×10^5. For the non-stationary wind whose mean wind speed increases from 13.5 m/s to 27 m/s, the Reynolds number varies between 1.47×10^5 and 2.94×10^5.

Symmetry boundary conditions are employed for the domain sides and top, while wall boundary conditions are used for the ground, stadium and surroundings. Rough wall-functions are applied to the ground with a roughness height of 6 m and roughness constant of 0.5, while all the others are treated as smooth walls. A pressure outlet is adopted at the outflow and the inlet condition is further detailed in the following.

As regard the grid size, cells measure approximately 6 m at the inlet, corresponding to a reasonably small fraction of the integral length scale of the approaching flow. In the proximity of the roof, cells measure 0.75m, corresponding to less than 1/200 the stadium overall size. No boundary layer cells are added to the roof surfaces, considering that the approaching flow is highly turbulent and thus, the presence of boundary layers is greatly disturbed by the incoming turbulence (y^+ mean/max is around 30/150, consistently with the adoption of wall-functions). An overview of the adopted mesh is depicted in Fig. 2. Overall, the mesh counts 8.5 M cells.

The adopted turbulence model is the well-known *k-equation*. Limited Gauss linear schemes are used for gradient and laplacian terms calculation, while LUST is adopted for advective terms appearing in the momentum conservation equations. Time advancement is obtained using the Crank–Nicolson scheme, while the PISO algorithm is used for pressure–velocity coupling. An Eurocode Category III profile is assumed with base velocity equal to 25 m/s, lading to a reference velocity at the roof height equal to 27 m/s. Overall, the total cells number is 8.5 million. The adopted time step is 0.012 s and simulations are allowed to evolve until initialization effect vanish and, then, advanced for 10 mins (for the stationary case). Simulations are performed in OpenFOAM version 6. The reader is invited to refer to [29] for further details.

3. Stationary and non-stationary inflows

3.1. Stationary inflows

When using LES, the first step in the evaluation of wind loads is the generation of appropriate inflow conditions. In this work, synthetic turbulence representative of that found in the ABL is generated relying on the PRFG[3] method, which allows to control the turbulence intensity of the three velocity components as well as nine integral length scale [30,31]. Additionally, the Variationally Based Inflow Correction, VBIC [32], procedure is adopted to moderate spurious pressure fluctuation generated due to incompatibility with boundary conditions confining with the inflow patch. The inflow generation procedure coincides with that already adopted in [29].

Fig. 3 reports the characterization of the velocity profiles sampled at the location where the stadium will be positioned, measured in empty domain conditions. The target wind profiles are reproduced with good accuracy. The mean wind speed at roof height, taken as 37 m above the ground, is 27 m/s. Indicating with u, v and w the along-wind, cross-wind and vertical velocity components, turbulence intensities at the reference height are $I_u = 20\%$, $I_v = 16\%$ and $I_w = 11\%$. Regarding the turbulence integral length scale, the values in the along wind, x direction, are 130 m, 60 m, and 40 m for the u, v and w components, respectively.

The spectra of the three velocity components measured in empty domain conditions at the stadium location are presented in Fig. 4, showing a good agreement with the target spectra.

A qualitative overview of the flow field obtained in the proximity of the roof is reported in Fig. 5. In particular, an overview of the flow in the surroundings can be seen in Fig. 5(a), the cavity flow is well-visible in Fig. 5(b), while an overview of the small-scale vortical structures generated by the stadium is reported in 5(c).

3.1.1. Non-stationary inflows

The generation of non-stationary inflows, for the sake of simplicity, follows as closely as possible the methodology adopted for the stationary case, reported in Section 3.1. In particular, in order to introduce the non-stationarity, the incoming mean velocity is modulated using a time-varying function, representing the time-evolution of the slowly varying mean wind speed. In other words, the logarithmic profile is kept unchanged in shape and equal to the one previously used for the stationary case, but its intensity is modulated in time.

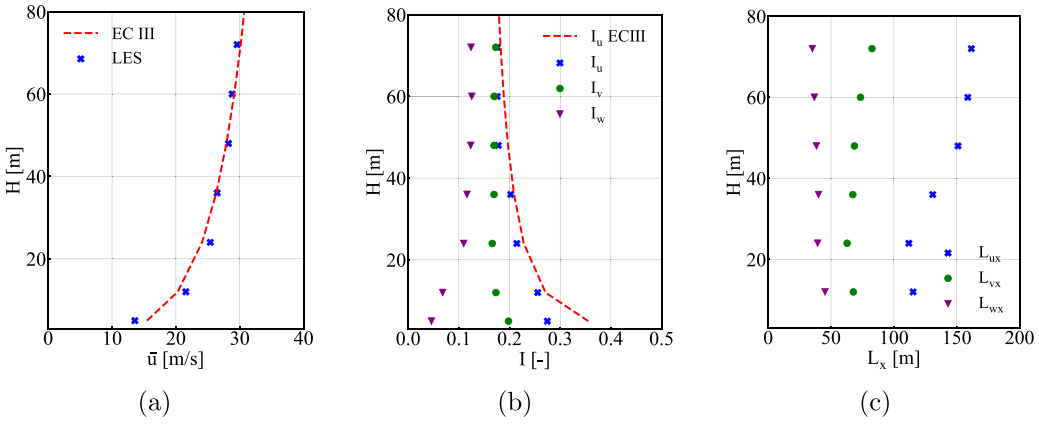

Fig. 3. Wind profiles for the stationary inflow conditions: (a) mean wind speed, (b) turbulence intensities and (c) turbulence integral length scales in the along wind direction.

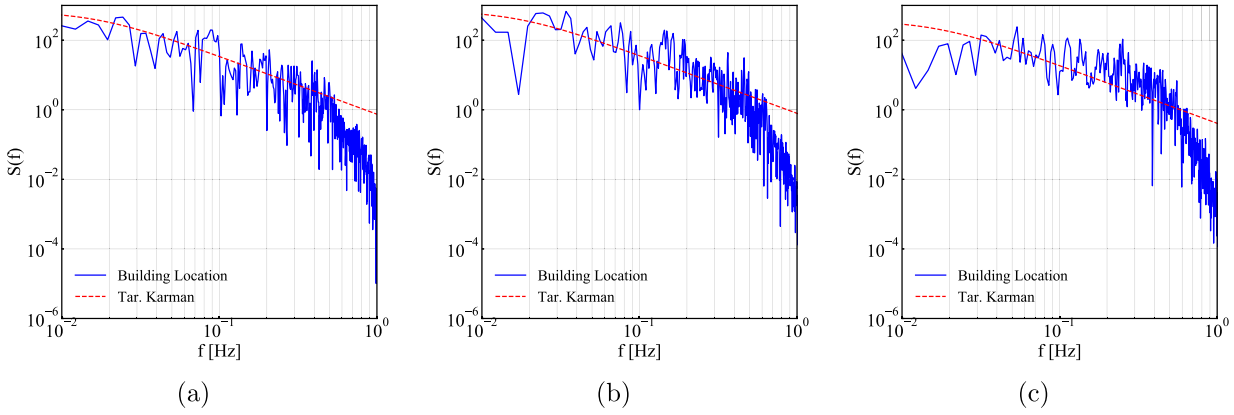

Fig. 4. Spectra of the three velocity components measured at the stadium location: (a) along-wind component, (b) cross-wind component and (c) vertical component.

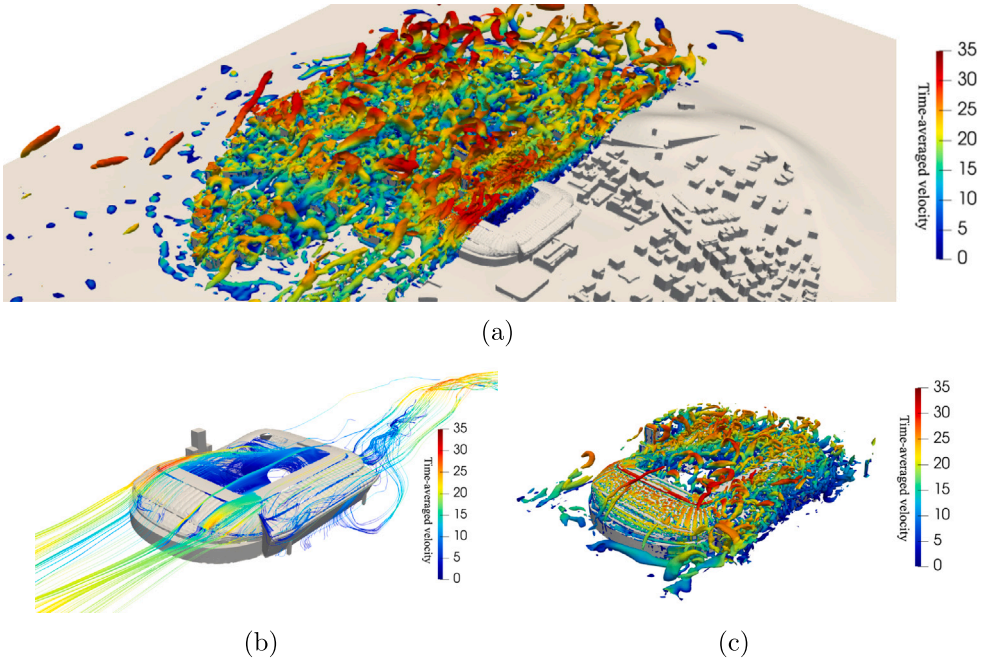

Fig. 5. Overview of the obtained velocity field in the proximity of the structure for stationary conditions: (a) overview of vorticity iso-surfaces, (b) streamlines and (c) close-up of vorticity iso-surfaces, coloured by mean velocity magnitude. (For interpretation of the references to colour in this figure legend, the reader is referred to the web version of this article.)

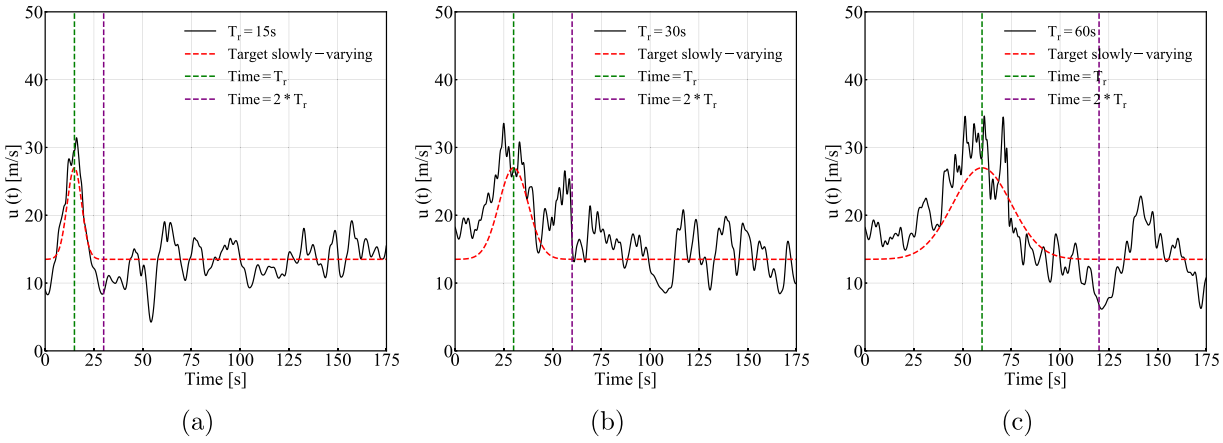

Fig. 6. Single realization of the non-stationary wind velocity at the stadium location in empty domain conditions (along-wind velocity component): (a) T_r = 15 s, (b) T_r = 30 s and (c) T_r = 60 s.

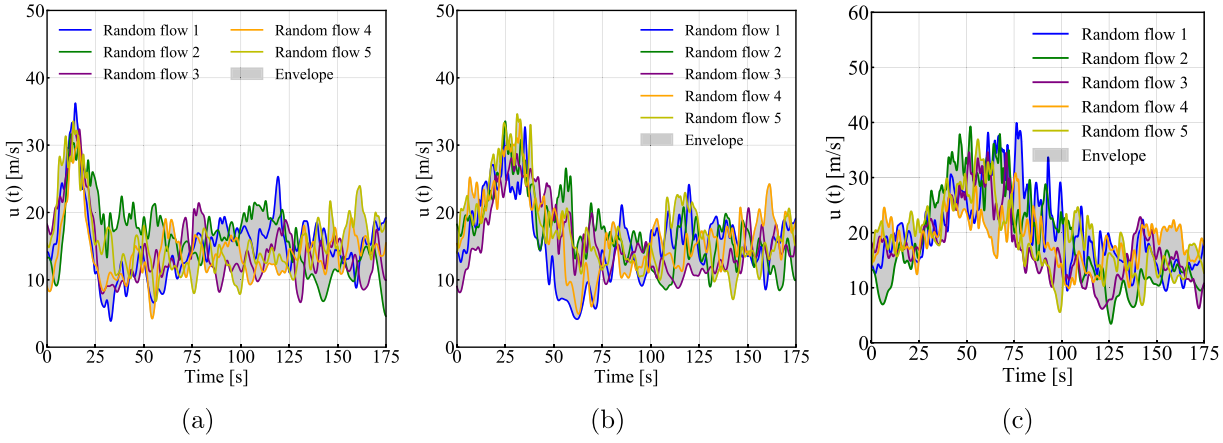

Fig. 7. Realizations of the non-stationary wind time-histories for different ramp-up times: (a) T_r = 15 s, (b) T_r = 30 s and (c) T_r = 60 s.

Numerous are the formulations available in the literature regarding the time evolution of the slowly-varying mean wind speed for downbursts and other non-stationary winds [15,33,34]. However, as pointed out by [35], the actual trends of different downbursts can vary significantly, with rump-up and decay times usually showing remarkable differences. A further factor to be taken into consideration is that usually downbursts superimpose onto standard background ABL flows.

In the present study, in order to keep the setup as simple as possible, the modulation function is chosen to be gaussian, so assuming equal ramp-up and decay times. Hereafter, we denote such rump-up and decay times as T_r, corresponding to 4 standard deviations of the aforementioned gaussian function. In addition, we fix the ratio between the maximum amplification of the velocity due to non-stationary effects with respect to the background ABL velocity and set it equal to 2.0. In particular, the time modulation function starts with a value equal to 0.5, reaches a value equal to 1.0 at T_r, and then decays again to 0.5. In such condition, as the peak value is equal to 1.0, the maximum reference dynamic pressure is equivalent to that of the stationary case previously discussed. Aiming at exploring non-stationary winds characterized by varying time-scale, we vary T_r so that it assumes values 15, 30 and 60 s.

As regards incoming turbulence, for the sake of simplicity, the same turbulent fluctuations used for the stationary flow are adopted for the non-stationary cases. We remark that the choice is deliberately over-simplified with respect to actual conditions expected during non-stationary wind events, leading to an overestimation of the turbulence intensity for the background ABL flow. Such aspect, despite being worth further investigation, is not expected to change substantially the outcome of the following analyses, in which the sudden change of the slowly varying mean wind speed dominates the response. A single realization of the non-stationary wind velocity at the stadium location for T_r = 15 s, 30 s, 60 s in empty domain conditions is shown in Fig. 6, together with the target slowly varying mean. As it can be noticed, a remarkable complication in the study of non-stationary flows using both experimental and numerical techniques is the impossibility to use time-averaging and ensemble-averaging in an interchangeable way, as the process is not ergodic.

We thus proceed to repeat the simulations multiple times, considering different realizations of the turbulent fluctuations. The different realizations are obtained varying the phases of the velocity-waves which compose the inflow, so providing different realizations while preserving the spectral content. Fig. 7 reports the along-wind velocity component in empty domain conditions for five realizations of the non-stationary flow at the stadium location.

Then, we extract the slowly varying mean calculating the ensemble average of the five realizations. The obtained results are presented in Fig. 8. It can be seen that overall, a reasonably good agreement is obtained between the recorded velocity and the target value, although some discrepancies between them can be clearly observed.

It is at this point important to notice that, due to the incompressibility constraint, differently from the real case, the velocity variations applied at the inflow are transmitted without delays to the roof location, see Fig. 6 (the time modulation function is applied at the inlet and effects are immediately transmitted at the stadium location). As a drawback, in the adopted setup, strong pressure variations develop

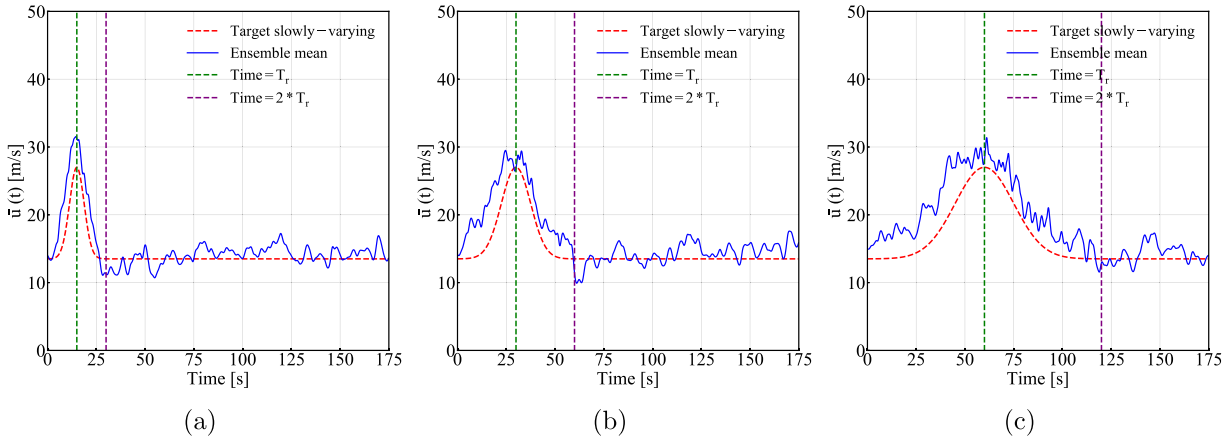

Fig. 8. Ensemble average of the 5 random realizations of the inflow for each T_r: (a) $T_r = 15$ s, (b) $T_r = 30$ s and (c) $T_r = 60$ s.

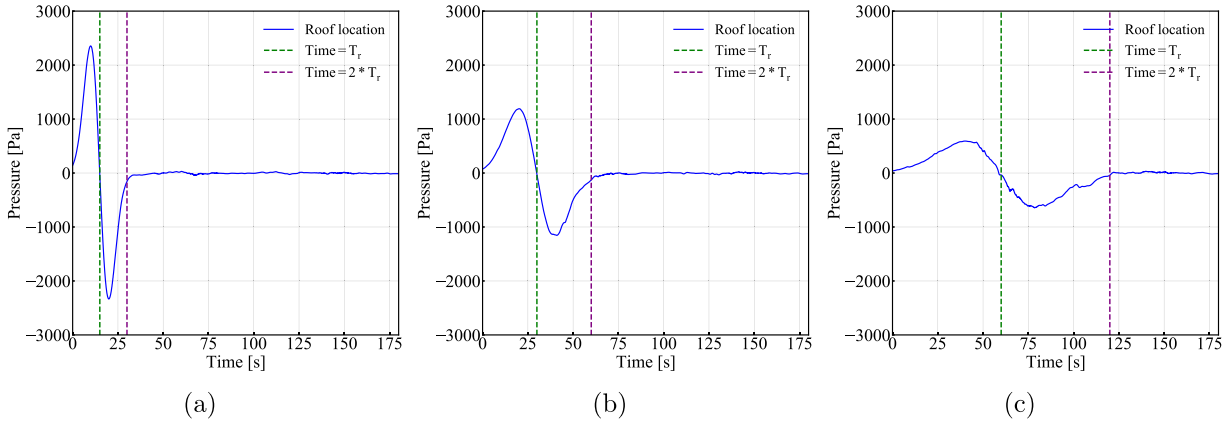

Fig. 9. Pressure time-histories at the stadium location: (a) $T_r = 15$ s, (b) $T_r = 30$ s and (c) $T_r = 60$ s.

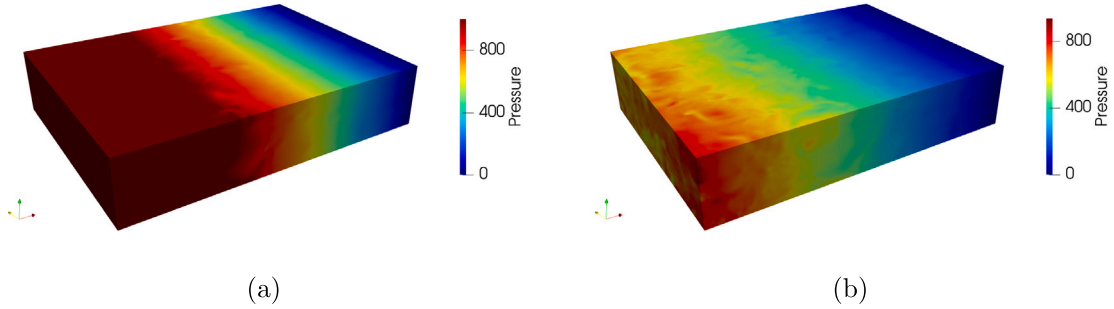

Fig. 10. Instantaneous pressure distributions: (a) $T_r = 30$ s and (b) $T_r = 60$ s.

during the rump-up and decay time, needed to accelerate and decelerate the flow. Such pressure variations superimpose to those induced by the incoming turbulence and induced by the structure itself and the surroundings. Fig. 9 reports such pressure variations, measured in empty domain conditions at the stadium location. As expected, the amplitude of the pressure variations increases with decreasing T_r. As it can be noticed in Fig. 10, such pressure variations are maximum at the inflow patch and vanish at the outflow, due to the zero pressure value boundary condition there imposed. More importantly, such static pressure fluctuations are coherent within the computational domain, so that their effect on the net pressure over immersed surfaces (like those composing the considered roof) is negligible.

We finally notice that, despite being eliminated in the calculation of net pressure, such fluctuation of the static pressure represent an undesirable feature of the adopted computational setup, based on confined flow conditions. Alternatives are represented by simulations of the downburst as a jet impinging on the ground [36,37] and the use of computational domains with an open-top, eventually using cylindrical periodicity for the side patches (to be better representative of the flow near the downburst centre). The authors experimented open-top and partially open-top boundary conditions, whose results are not here reported for the sake of brevity, concluding that pressure fluctuations could be only partially moderated. As a drawback such boundary conditions led to heavy modifications of the slowly varying mean wind speed applied at the inflow when proceeding towards the outflow (with a substantial portion of the volume injected at the inflow leaving the computational domain from the top patch in the proximity of the inflow). Such undesired modifications intensify with decreasing T_r, so that the inflow characterized by $T_r = 15$ was completely altered when

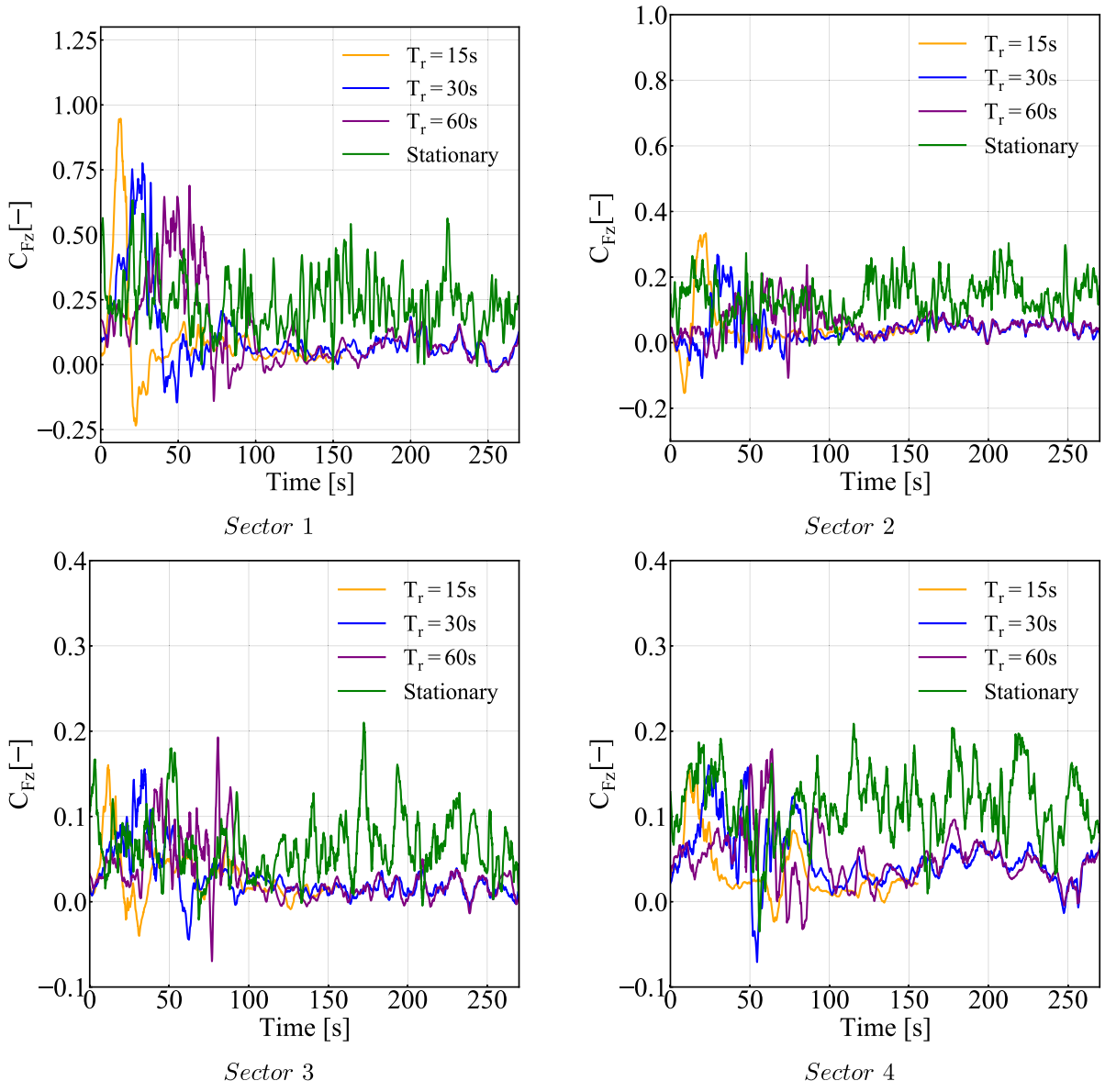

Fig. 11. The force coefficients time-histories for stationary and non-stationary cases.

reaching the stadium location. Due to such reasons, confined conditions have been retained for the present study.

4. Wind loads

We now consider the forces exerted over the stadium roof during the non-stationary wind event, and compare them to results obtained in the stationary case. In particular, the vertical wind force (F_z) is calculated by integrating the net pressure acting on the roof and it is considered to be positive upward. We thus have $C_{Fz} = F_z/(0.5\rho\bar{U}_{ref}^2 A_{ref})$ where C_{Fz} is the vertical force coefficient, A_{ref} is the reference area of each roof sector, ρ is the air density and U_{ref} is the reference velocity measured at roof height at the stadium location in empty domain conditions. U_{ref} is taken as the time-averaged velocity for the stationary case and as the maximum (in time) of the ensemble-averaged wind speed reported in Fig. 8 for the non-stationary case, in order to allow for a fair comparison of the results.

In particular, Fig. 11 reports C_{Fz} time histories, for each sector of the stadium roof (as reported in Fig. 1(b)), aerodynamic coefficients related to the vertical force. Note that, as expected, C_{Fz} reaches a peak value in correspondence of the peak of the slowly-varying mean wind speed and, then, decreases to much lower values. Turbulent fluctuations render the inspection of the obtained results not straightforward. Nevertheless, clear trends emerge: for Sectors 3 and 4 it appears that the extreme values reached in the non-stationary simulations are well-comparable to those found in the stationary case. This also confirms, as expected, that the calculation of the net pressure is not influenced by the variability of the static pressure discussed in Section 3.1.1. For Sector 2, which is the one located upstream, a trend is noticed, with unsteady aerodynamic effects leading to stronger aerodynamic forces as T_r is decreased. Despite such trend, aerodynamic forces are anyway well-comparable to those measured in stationary conditions. Finally, for Sector 1, corresponding to the downstream sector of the roof, we notice a remarkable and systematic increase of the aerodynamic forces as T_r is decreased, reaching values well-above the extremes found in the stationary case. Such increase appears to be noticeable, but relatively small for $T_r = 60$, and becomes relevant for $T_r = 15$.

To further emphasize the result, the running mean of the signals shown in Fig. 11 is reported in Fig. 12, using a time window of 3 s to eliminate short-time-scale oscillations. In the figure, we also report the mean and 99.7% gaussian confidence interval for the stationary

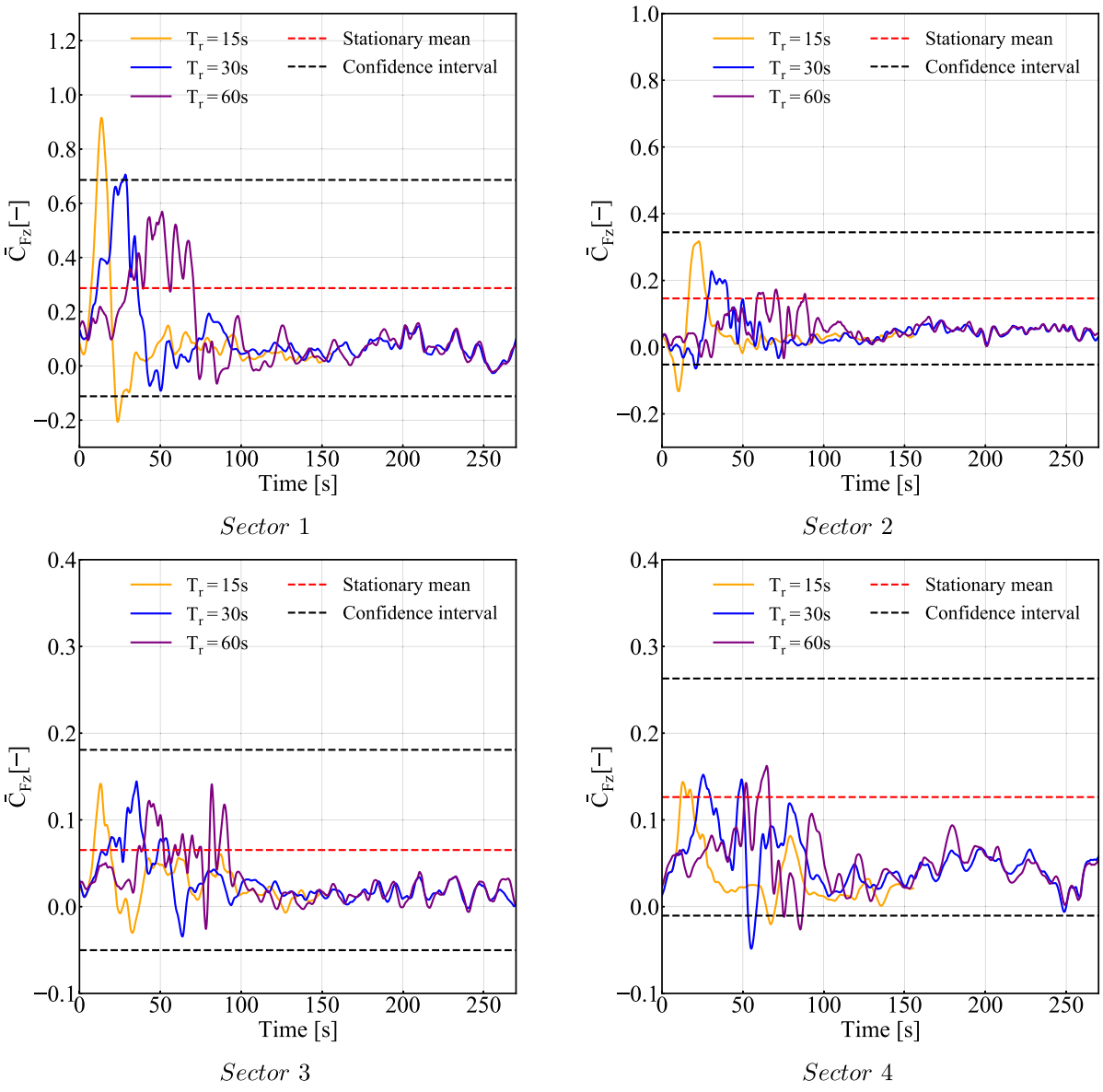

Fig. 12. The running mean of the force coefficients time-histories for stationary and non-stationary cases.

case (i.e. three standard deviations, no running mean applied). We remark that such confidence intervals shall be taken with a grain of salt as, in general C_{Fz} is not expected to follow a gaussian distribution. Despite such limitations, it clearly emerges that for Sectors 3 and 4, the obtained results do not deviate from the extremes measured in the stationary case in a remarkable way. For such cases the simple analyses here performed do not allow to draw final conclusions on the role of unsteady aerodynamic effects.

Also for Sector 2 the presented simple analyses do not allow to reach final conclusions, but clear trends can be identified with varying T_r. The aerodynamic response appears to be characterized by an initial decrease of the uplift force, followed by a robust increase, with extreme values inversely proportional to T_r.

Finally, for Sector 1, a clear trend can be identified with varying T_r: the aerodynamic response is initially characterized by a strong uplift, followed by a rapid decrease in the wind force. The intensity of the response is clearly inversely proportional to T_r, and for $T_r = 15$ forces exceed the confidence interval on both the positive and negative sides, pointing to the presence of unsteady aerodynamic effects. As the sector affected by such increase in aerodynamic load is the downstream one, is can be expected that the behaviour is governed by the shedding of large vortices from the upstream part or by a dynamic excitation of the shear layers detached by the upstream sector.

In particular, the instantaneous net pressure distribution over the roof at the maximum lift condition is reported in Fig. 13. It shall be recalled that, for the stationary case (reported in Fig. 13(a)), a time history of 10 min has been simulated and the reported pressure distribution is the one corresponding to the maximum lift within such interval. For the non-stationary cases instead, the maximum lift is always recorded in proximity of the maximum gust speed. It can be clearly seen that the net pressure values are well-comparable between the four cases, confirming the fact that net pressures can be safely measured also in presence of strong static pressure fluctuations, without introducing undesirable effects. The maximum suctions for the stationary case appears to be the strongest recorded within all the four presented cases and the corresponding pressure distribution shows to be clearly non-symmetric (here intending the overall distribution, disregarding small-scale fluctuations), which is expected considering that gusts generated by the incoming flow and the surroundings control the lift generation and those are generally not aligned with the mean flow. The non-stationary cases characterized by $T_r = 30$ and $T_r = 60$ are qualitatively similar to the stationary case, with comparable or

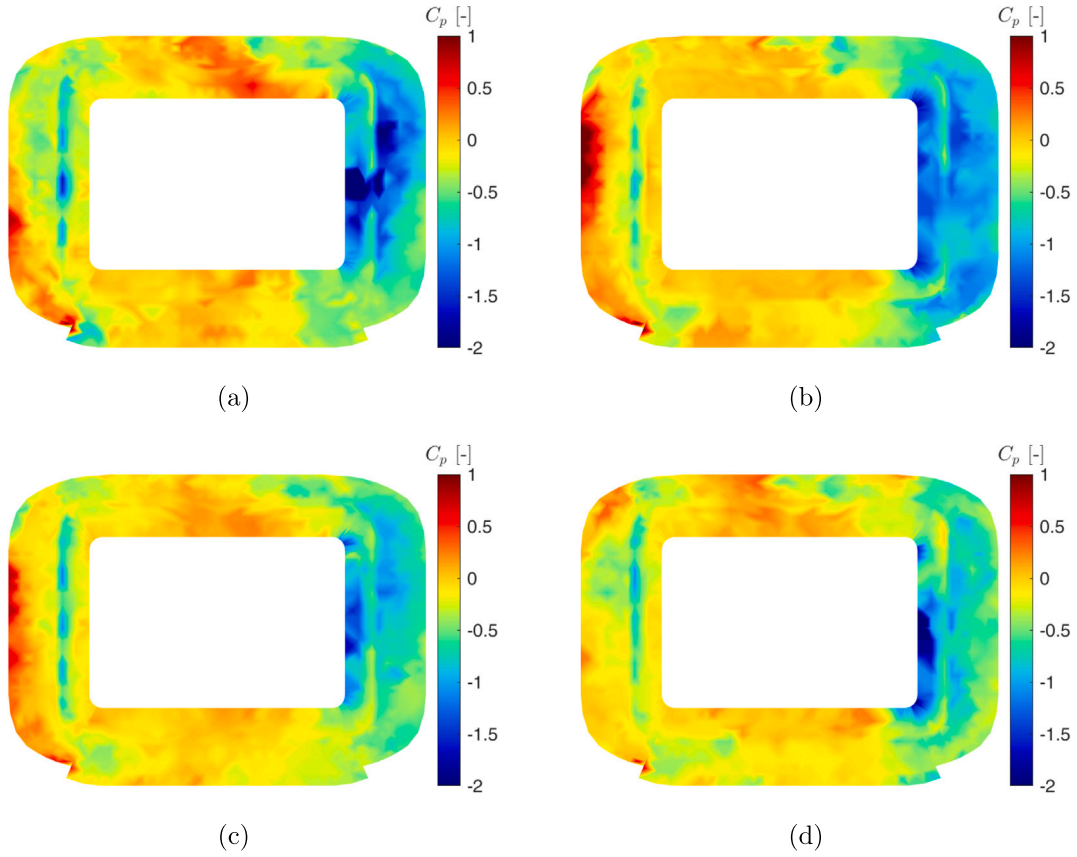

Fig. 13. Instantaneous net pressure coefficient distributions over the roos at the maximum uplift condition: (a) stationary, (b) T_r = 15 s, (c) T_r = 30 s, (d) T_r = 60 s (values have been clipped to the range [−2.50, 1.00] to enhance readability, actual values are in the range [−3.39, 1.04]).

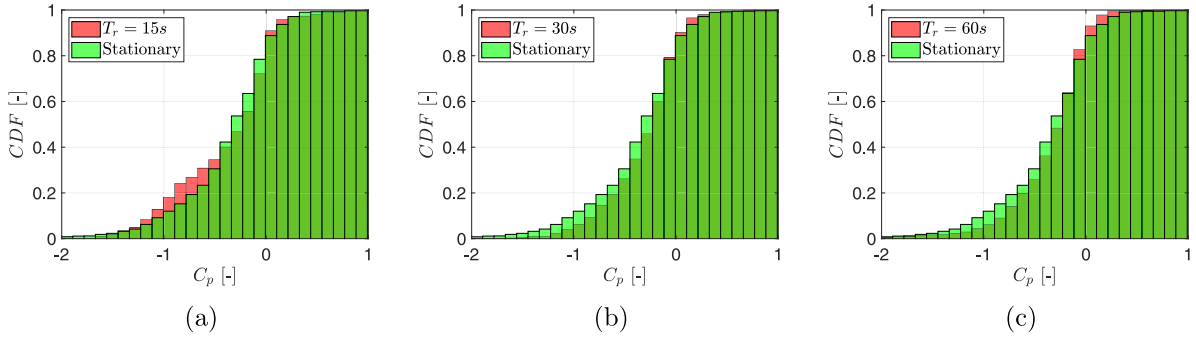

Fig. 14. Cumulative Density Function of the net pressure coefficient over Sector 1: (a) T_r = 15 s and (b) T_r = 30 s and (c) T_r = 60 s.

weaker negative and positive pressures. Finally, T_r = 15 appear to have a slightly more symmetric distribution (which is expected as the flow is controlled by the mean flow variation), with peak suctions weaker than the stationary case but a more uniform distribution over Sector 1. Fig. 14 shows the Cumulative Density Function, CDF, of the net pressure over Sector 1 at the maximum lift instant (the same depicted in Fig. 13). It can be noticed that only for T_r = 15 the CDF of the non-stationary case is significantly higher than the stationary one, showing a hump in the zone characterized by C_p in the range [−1.0,−0.5]. Overall, it can be concluded that while T_r = 30 and T_r = 60 lead to conditions which are comparable to the worst one measured in the stationary case, T_r = 15 shows an increase of the average suctions in the downstream sector, so leading to an overall larger lift value.

For the sake of completeness, in Fig. 15 we report the time-averaged net pressure distribution over the roof for the stationary case, as well as its CDF for Sector 1 and the CDF previously presented for T_r = 15 s. As expected, the two CDFs show a remarkable qualitative difference (they cannot be matched by an appropriate re-scaling), indicating that the previously observed lift overshooting cannot be reproduced by the introduction of a properly calibrated gust factor. This evidence further confirms that the observed lift overshooting is related to the unsteady aerodynamic behaviour of the flow and is controlled by the non-stationary character of the slowly varying mean flow.

We finally notice that, in the proposed simulations, due to the incompressibility constraint, the gust invests the whole structure instantaneously, which might be not completely representative of real operating conditions. The difference is similar to that between the well-known Kussner and Wagner functions [24], appearing in airfoil theory. Despite such limitations, results show clear evidence of an intensification of the aerodynamic loads on the downstream sector of the roof, mainly limited to cases in which T_r < 30 s. It should be noticed that, despite being the present study focused on ABL flow conditions,

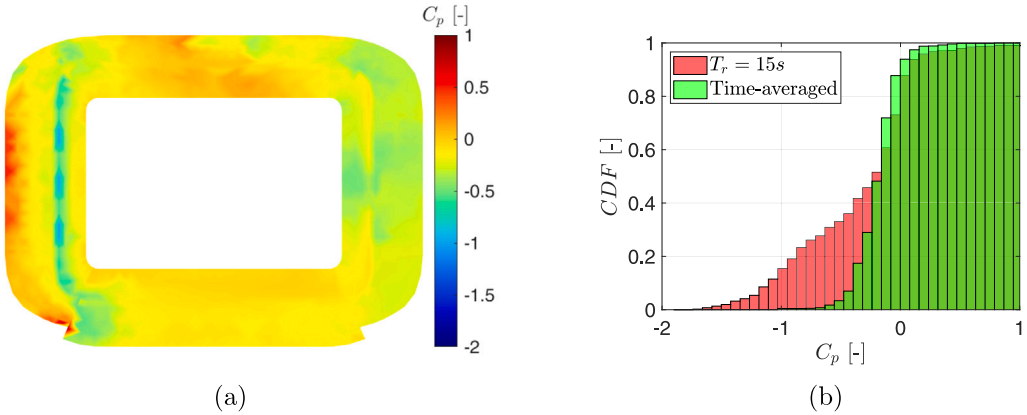

Fig. 15. Time-averaged net pressure for the stationary case: (a) distribution and (b) Cumulative Density Function over Sector 1.

given the short T_r needed to observe the phenomenon, the role of turbulence in the incoming flow is expected to be marginal for its development.

5. Conclusions

In the present paper, an evaluation of the role played by unsteady aerodynamic effects in the definition of wind loads for large-span partially-open roofs has been provided. The goal was to isolate unsteady aerodynamic effects from other factors, which typically characterize non-stationary winds such as, for instance, modifications of the standard ABL velocity profiles and the impulsive nature of the structural response. Numerical simulations performed with LES highlighted difficulties in controlling the shape and intensity of the velocity field impinging on the roof, due to modifications of the velocity field applied at the inflow during its transmission within the computational domain. In order to minimize such undesired modifications, simulations have been performed in confined flow conditions which, however, inevitably leads to strong variations of the static pressure within the computational domain. Despite undesirable, such aspects did not appear to be critical for the present investigation. Results indicate that unsteady aerodynamic effects might lead to load intensifications on the downstream sectors of large-span partially-open stadium roofs for non-stationary wind events with rump-up/decay time shorter than approximately 30 s. Inspecting the pressure distribution, it has been shown that the phenomenon is related to an overall increase of the suctions over the sector, rather than localized strong depressions. As expected, evidences point to the impossibility to explain such increase in the lift coefficient to the quasi-static behaviour of the roof, indicating the necessity to consider unsteady aerodynamic effects to account for such effects. Further research shall individuate the aerodynamic mechanisms underlying such result, possibly relying on simpler models with respect to the one used in this study. Research on the matter is still extremely scarce and further efforts are needed in order to confirm the results of the present study as well as evaluating the actual importance of such results in terms of design wind loads, which requires to enlarge the number of studied configurations and properly account for all peculiarities of non-stationary wind events.

CRediT authorship contribution statement

Jin Xing: Investigation, Writing – original draft. **Luca Patruno:** Conceptualization, Formal analysis, Methodology, Writing – review & editing. **Stefano de Miranda:** Funding acquisition. **Francesco Ubertini:** Funding acquisition.

Declaration of competing interest

The authors declare that they have no known competing financial interests or personal relationships that could have appeared to influence the work reported in this paper.

References

[1] Theodore Fujita T. Downbursts: meteorological features and wind field characteristics. J Wind Eng Ind Aerodyn 1990;36:75–86, URL https://www.sciencedirect.com/science/article/pii/016761059090294M. The Sixth U.S. National Conference on Wind Engineering.
[2] Tamura Y, Shimada K, Hibi K. Wind response of a tower (typhoon observation at the nagasaki Huis Ten bosch domtoren). J Wind Eng Ind Aerodyn 1993;50:309–18, URL https://www.sciencedirect.com/science/article/pii/0167610593900864.
[3] Schroeder JL, Smith DA, Peterson RE. Variation of turbulence intensities and integral scales during the passage of a hurricane. J Wind Eng Ind Aerodyn 1998;77–78:65–72, URL https://www.sciencedirect.com/science/article/pii/S0167610598001329.
[4] Twisdale LA, Vickery PJ. Research on thunderstorm wind design parameters. J Wind Eng Ind Aerodyn 1992;41(1):545–56, URL https://www.sciencedirect.com/science/article/pii/016761059290461I.
[5] Gomes L, Vickery B. Extreme wind speeds in mixed wind climates. J Wind Eng Ind Aerodyn 1978;2(4):331–44, URL https://www.sciencedirect.com/science/article/pii/0167610578900181.
[6] Solari G. Thunderstorm downbursts and wind loading of structures: Progress and prospect. Front Built Environ 2020;6:63.
[7] Goff RC. Vertical structure of thunderstorm outflows. Mon Weather Rev 1976;104(11):1429–40, URL https://journals.ametsoc.org/view/journals/mwre/104/11/1520-0493_1976_104_1429_vsoto_2_0_co_2.xml.
[8] Canepa F, Burlando M, Solari G. Vertical profile characteristics of thunderstorm outflows. J Wind Eng Ind Aerodyn 2020;206:104332, URL https://www.sciencedirect.com/science/article/pii/S0167610520302427.
[9] Li Y, Mason MS, Bin H-Y, Lo Y-L. Aerodynamic characteristics of a high-rise building in a steady thunderstorm outflow-like flow field. J Wind Eng Ind Aerodyn 2023;240:105501.
[10] Chay M, Letchford C. Pressure distributions on a cube in a simulated thunderstorm downburst—Part A: stationary downburst observations. J Wind Eng Ind Aerodyn 2002;90(7):711–32.
[11] Jubayer C, Romanic D, Hangan H. Aerodynamic loading of a typical low-rise building for an experimental stationary and non-Gaussian impinging jet. Wind Struct Int J 2019;28(5):315–29, Cited by: 11.
[12] Lombardo FT, Smith DA, Schroeder JL, Mehta KC. Thunderstorm characteristics of importance to wind engineering. J Wind Eng Ind Aerodyn 2014;125:121–32, URL https://www.sciencedirect.com/science/article/pii/S0167610513002791.
[13] Kijewski-Correa T, Bentz A. Wind-induced vibrations of buildings: role of transient events. Proc Inst Civ Eng - Struct Build 2011;164(4):273–84, arXiv: https://doi.org/10.1680/stbu.2011.164.4.273.
[14] Brusco S, Buresti G, Piccardo G. Thunderstorm-induced mean wind velocities and accelerations through the continuous wavelet transform. J Wind Eng Ind Aerodyn 2022;221:104886.
[15] Kwon D-K, Kareem A. Gust-front factor: New framework for wind load effects on structures. J Struct Eng 2009;135(6):717–32.
[16] Kwon DK, Kareem A. Towards codification of thunderstorm/downburst using gust front factor: Model-based and data-driven perspectives. Eng Struct 2019;199:109608.

[17] Le T-H, Caracoglia L. Modeling vortex-shedding effects for the stochastic response of tall buildings in non-synoptic winds. J Fluids Struct 2016;61:461–91, URL https://www.sciencedirect.com/science/article/pii/S0889974615002893.
[18] Chen X. Analysis of alongwind tall building response to transient nonstationary winds. J Struct Eng 2008;134(5):782–91.
[19] Hao J, Wu T. Nonsynoptic wind-induced transient effects on linear bridge aerodynamics. J Eng Mech 2017;143(9):04017092.
[20] Le T-H, Caracoglia L. Modeling vortex-shedding effects for the stochastic response of tall buildings in non-synoptic winds. J Fluids Struct 2016;61:461–91.
[21] Brusco S, Solari G. Transient aeroelasticity of structures subjected to thunderstorm outflows. Eng Struct 2021;245:112801.
[22] Brusco S, Bin H-Y, Lo Y-L, Piccardo G. Transient aerodynamics of a square cylinder under downburst-like accelerating flows reproduced in a multiple-fan wind tunnel. J Fluids Struct 2024;124:104038.
[23] Takeuchi T, Maeda J. Unsteady wind force on an elliptic cylinder subjected to a short-rise-time gust from steady flow. J Wind Eng Ind Aerodyn 2013;122:138–45, URL https://www.sciencedirect.com/science/article/pii/S0167610513001232. The Seventh International Colloquium on Bluff Body Aerodynamics and Applications (BBAA7).
[24] Scanlan RH. Problematics in formulation of wind-force models for bridge decks. J Eng Mech 1993;119(7):1353–75.
[25] Scanlan RH, Béliveau J-G, Budlong KS. Indicial aerodynamic functions for bridge decks. J Eng Mech Div 1974;100(4):657–72.
[26] Lee T, Budwig R. The onset and development of circular-cylinder vortex wakes in uniformly accelerating flows. J Fluid Mech 1991;232:611–27.
[27] Yang T, Mason MS. Aerodynamic characteristics of rectangular cylinders in steady and accelerating wind flow. J Fluids Struct 2019;90:246–62, URL https://www.sciencedirect.com/science/article/pii/S0889974618309320.
[28] Le V, Caracoglia L. Experimental investigation on non-stationary wind loading effects generated with a multi-blade flow device. J Fluids Struct 2020;96:103049.
[29] Xing J, Patruno L, de Miranda S, Pinardi S, Majowiecki M, Ubertini F. Early stages wind load assessment using computational fluid dynamics: The new bologna stadium roof. Structures 2023;47:1912–26.
[30] Patruno L, Ricci M. On the generation of synthetic divergence-free homogeneous anisotropic turbulence. Comput Methods Appl Mech Engrg 2017;315:396–417.
[31] Patruno L, Ricci M. A systematic approach to the generation of synthetic turbulence using spectral methods. Comput Methods Appl Mech Engrg 2018;340:881–904.
[32] Patruno L, de Miranda S. Unsteady inflow conditions: A variationally based solution to the insurgence of pressure fluctuations. Comput Methods Appl Mech Engrg 2020;363:112894, URL https://www.sciencedirect.com/science/article/pii/S0045782520300761.
[33] Abd-Elaal E-S, Mills JE, Ma X. Empirical models for predicting unsteady-state downburst wind speeds. J Wind Eng Ind Aerodyn 2014;129:49–63, URL https://www.sciencedirect.com/science/article/pii/S0167610514000622.
[34] Hjelmfelt MR. Structure and life cycle of microburst outflows observed in colorado. J Appl Meteorol Climatol 1988;27(8):900–27.
[35] Solari G, Burlando M, De Gaetano P, Repetto MP. Characteristics of thunderstorms relevant to the wind loading of structures. Wind Struct 2015;20(6):763–91.
[36] Mason M, Wood G, Fletcher D. Impinging jet simulation of stationary downburst flow over topography. Wind Struct 2007;10(5):437–62.
[37] Žužul J, Ricci A, Burlando M, Blocken B, Solari G. CFD analysis of the windeee dome produced downburst-like winds. J Wind Eng Ind Aerodyn 2023;232:105268.